



POLİTEKNİK DERGİSİ

JOURNAL of POLYTECHNIC

ISSN:1302-0900 (PRINT), ISSN: 2147-9429 (ONLINE)

URL: <http://dergipark.org.tr/politeknik>



Analysis of structure-property relationship for an anthelmintic drug, Mebendazole nitrate salt, using density functional theory approach

Yoğunluk fonksiyonel teorisi yaklaşımı kullanılarak antelmintik bir ilaç olan mebendazol nitrat tuzu için yapı-özellik ilişkisinin analizi

Yazar(lar) (Author(s)): Akansha TYAGI¹, Anuj KUMAR²

ORCID¹: 0000-0002-7815-8380

ORCID²: 0000-0002-3143-7761

Bu makaleye şu şekilde atıfta bulunabilirsiniz(Tocitetothisarticle): Tyagi A., Kumar A., "Analysis of Structure-property relationship for an anthelmintic drug, mebendazole nitrate salt, using density functional theory approach", *Politeknik Dergisi*, 25(3): 1055-1067, (2022).

Erişim linki(To link to this article):<http://dergipark.org.tr/politeknik/archive>

DOI: 10.2339/politeknik.828211

Analysis of Structure-Property Relationship for an Anthelmintic Drug, Mebendazole Nitrate Salt, using Density Functional Theory Approach

Highlights

- ❖ DFT calculations at B3LYP level allowed a better reproduction of the experimental geometry.
- ❖ The scaled and experimental FTIR spectra have been compared.
- ❖ NBO analysis provided information on intra-molecular electron delocalization.
- ❖ MEP surface shows several possible sites for electrophilic/nucleophilic attack.
- ❖ Large affinity value confirms strong biological activity of MBZ-N ligand with protein and its possible potential application as a drug.

Graphical Abstract

In this study theoretical investigation on structural, spectroscopic and electronic behaviour of Mebendazole nitrate salt is reported.

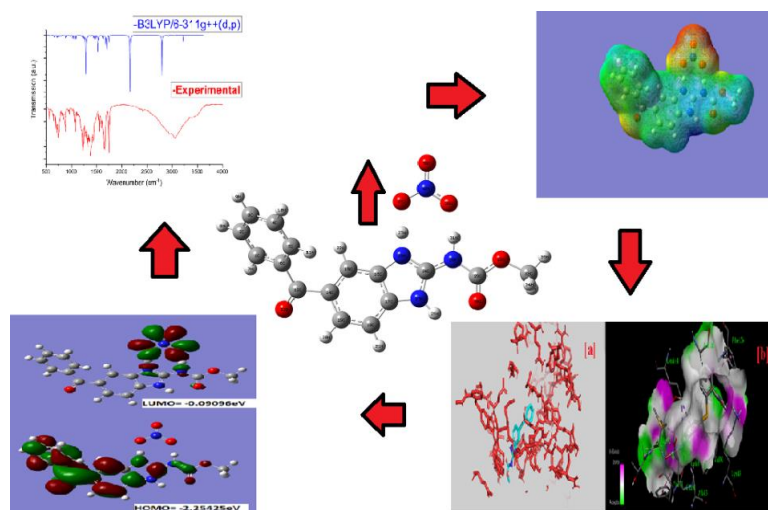


Figure. Graphical abstract of study

Aim

To investigate the structural, spectroscopic and biological properties of Mebendazole nitrate salt.

Design & Methodology

All the calculations are done using Density Functional Theory at B3LYP method with 6-311++G(d,p) basis set by Gaussian 09 program package.

Originality

Mebendazole nitrate salt has never been examined at the electronic level, The work reported is new and original.

Findings The detailed PED analysis made possible an unambiguous assignments of the modes in vibrational spectra. The molecular reactivity analysis of NBO, HOMO-LUMO and MEP gave an insight into the possible biological activities.

Conclusion

Molecular docking study of the MBZ-N molecule with Tyrosine-protein kinase ABL has shown strong ligand receptor activity which confirms the pharmacological application of MBZ-N molecule)

Declaration of Ethical Standards

The author(s) of this article declare that the materials and methods used in this study do not require ethical committee permission and/or legal-special permission.

Analysis of Structure-Property Relationship for an Anthelmintic Drug, Mebendazole Nitrate Salt, using Density Functional Theory Approach

Araştırma Makalesi / Research Article

Akansha TYAGI, Anuj KUMAR*

Chaudhary Charan Singh University- Physics Department, 250004, Meerut, India

(Geliş/Received : 20.10.2020 ; Kabul/Accepted : 01.04.2021 ; Erken Görünüm/Early View : 21.04.2021)

ABSTRACT

Various multicomponent of Mebendazole , (5-benzoyl-1H-benzimidazole- 2-yl)-carbamic acid methyl ester) (MBZ), are recognised by WHO as a synthetic anthelmintic drug. These multicomponent molecules show differences in their properties, mainly in their solubility and efficacy in controlling worm infections. These differences may be assigned to different structure of these multicomponents. Understanding of structure property relationship using theoretical investigations may provide us a way to synthesise new multicomponent of MBZ and estimating their properties. Therefore, here we report electronic and spectroscopic investigations on a new MBZ multicomponent Active Pharmaceutical Ingredient (API) Mebendazole nitrate salt (MBZ-N) using Density functional theory (DFT) approach. Becke's three- parameter hybrid functional (B3LYP) method has been used for all computations with 6-311++G(d,p) basis set, which gives the best compromise between accuracy and computational cost.Optimized geometry was further used for the calculation of vibrational spectra and molecular reactivity properties analysis such as natural bond analysis (NBO), HOMO-LUMO, and Molecular Electrostatic Potential (MEP). To understand its biological activity such as protein inhibiting, the molecular docking study of the MBZ-N molecule with Tyrosine-protein kinase ABL is also reported.

Keywords: Mebendazole, DFT, vibrational spectra, NBO.

Yoğunluk Fonksiyonel Teorisi Yaklaşımı Kullanılarak Antelmintik Bir İlaç Olan Mebendazol Nitrat Tuzu için Yapı-Özellik İlişkisinin Analizi

ÖZ

Mebendazole, (5-benzoil-1H-benzimidazol-2-il) -karbamik asit metil ester) (MBZ) 'nin çeşitli çoklu bileşenleri, WHO tarafından sentetik bir antelmintik ilaç olarak kabul edilmektedir. Bu çok bileşenli moleküller, özelliklerinde, özellikle çözünürlüklerinde ve solucan enfeksiyonlarını kontrol etmedeki etkinliklerinde farklılıklar gösterir. Bu farklılıklar, bu çoklu bileşenlerin farklı yapılarına atanabilir. Teorik araştırmalar kullanılarak yapı özelliği ilişkisinin anlaşılması, bize MBZ'nin yeni çoklu bileşenini sentezlemek ve özelliklerini tahmin etmek için bir yol sağlayabilir. Bu nedenle, burada, Yoğunluk fonksiyonel teorisi (DFT) yaklaşımını kullanarak yeni bir MBZ çok bileşenli Aktif Farmasötik Bileşen (API) Mebendazol nitrat tuzu (MBZ-N) üzerine elektronik ve spektroskopik araştırmaları rapor ediyoruz. Becke'nin üç parametreli hibrit işlevsel (B3LYP) yöntemi, doğruluk ve hesaplama maliyeti arasında en iyi uzaşmayı sağlayan 6-311 ++ G (d, p) temel setine sahip tüm hesaplamalar için kullanılmıştır. doğal bağ analizi (NBO), HOMO-LUMO ve Moleküler Elektrostatik Potansiyel (MEP) gibi titreşim spektrumları ve moleküler reaktivite özellikleri analizi. Protein inhibe etme gibi bilojik aktivitesini anlamak için, MBZ-N molekülünün Tirozin-protein kinaz ABL ile moleküler kenetlenme çalışması da rapor edilmiştir.

Anahtar Kelimeler: Mebendazole, DFT, titreşim spektrumları, NBO.

1. INTRODUCTION

Theoretical investigations are the very useful approach to understand the structure-property relationship and prediction of the properties of existing and proposed drug molecules. In the last decade density functional theory (DFT) has emerged as an important tool to understand the spectroscopic, electronic, optical and biological etc. properties of the molecules. It is established fact that the properties of materials are closely related to their molecular structure. Computational studies such as potential energy

distribution(PED) in vibrational modes, natural bond analysis (NBO), HOMO-LUMO, Molecular Electrostatic Potential (MEP), and Molecular docking can help to understand and interpret the observed experimental properties of the known materials at molecular as well as electronic level. Similarly, they may also predict properties of a proposed material. This understanding open up new ways for the discovery of new materials with desired properties.

The Mebendazole (MBZ), (5-benzoyl-1H-benzimidazole-2-yl)-carbamic acid methyl ester is a potent drug for controlling worm infections [1]. MBZ is also listed in the World Health Organization's Model

Sorumlu yazar (Corresponding Author)

e-mail : dranujkumarccsu@gmail.com

List of Essential Medicines [2]. It has three A, B and C polymorphic forms [3] having different solubility in water[4]. Form A is the most stable [5], but has lower solubility. Therefore, many multicomponent structures from pure polymorph A has been synthesized and studied for fiding a better therapeutic activity level and greater solubility[6-8]. Recently, new MBZ multicomponent, Mebendazole nitrate salt (MBZ-N) has been synthesized by Eduardo L. Gutierrez et al.[9].

To the best of our knowledge Mebendazole nitrate salt (MBZ-N) has not been investigated at theoretical level. Therefore, in the present work we report computational investigations on the structure, vibrational spectra, and molecular reactivity indicators such as natural bond analysis (NBO), HOMO-LUMO and Molecular Electrostatic Potential (MEP) for getting insight of the title molecule MBZ-N at the atomic and electronic level. To understand its biological activity such as protein inhibiting, the molecular docking study of the MBZ-N molecule with Tyrosine-protein kinase ABL is also reported.

2. COMPUTATIONAL DETAILS

The molecular geometry optimization, vibrational wavenumbers calculations, NBO and HOMO-LUMO analyses of the MBZ-N molecule have been done using DFT approach with the Gaussian 09W program package [10].Becke's three-parameter hybrid functional (B3LYP) method has been used for all computations with 6-311++G(d,p) basis set, which gives the best compromise between accuracy and computational cost.The vibrational (IR and Raman) spectra and wavenumbers have been computed based on the optimized molecular structure of the compound in the gas phase. The vibrational band assignments have been performed in terms of PED using GAR2PED program [11]. The internal coordinates was defined using Pulay's recommendations [12].The Natural Bond Orbital (NBO) calculations were done by NBO 5.0 Program built in the Gaussian 09W package at B3LYP/6-31G+(d,p) level.NBO analysis helps us in understanding various second order interactions,which are the measure of the intramolecular delocalization or hyper conjugation, between the filled orbital of one subsystem and vacant orbital of another subsystem. The highest occupied and lowest unoccupied molecular orbitals (HOMO and LUMO) of the compound were analyzed. The MEP surface has been imitated using the optimized molecular geometry (in a vacuum) of the MBZ-N. AutoDockVina program [13]was used to perform molecular docking analyses.

3. RESULTS AND DISCUSSION

3.1. Molecular geometry

Molecular geometry was fully optimized by Berny's optimization algorithm using redundant internal co-

ordinates. At the optimized structure of the title molecule no imaginary frequency modes were obtained, proving that a true minimum on the potential energy surface. The optimum geometry was determined by minimizing the energy with respect to all geometrical parameters without



Figure 1. Optimized molecular structure of MBZ-N at B3LYP/6-311++G(d,p) level.

imposing molecular symmetry constraints.

The optimized molecular structure of MBZ-N obtained from GAUSSIAN 09W program, calculated at B3LYP 6-311++G(d,p) is shown in Figure 1. The geometrical parameters such as bond lengths, bond angles and dihedral angles obtained from optimized MBZ-N structure compared with experimental values [9]are presented in Table1.

Mebendazole nitrate salt (MBZ-N) mainly has two benzene rings, one diazole ring and a nitrate group. Out of these two benzene rings, one ring is independent and the other is joined with diazole moiety. Due to the presence of NO_3 group, the structure of MBZ-N may be subjected to hydrogen bonding. The optimized structural parameters, in general, are in good agreement with the experimental data except slight deviation observed for few bond lengths and torsions.These discrepancies in structural parameters may be associated to isolated molecule model used for calculations, and therefore, intermolecular interactions in unit cell are not taken into consideration.Close examination of calculated values in comparison to experimental results reveals that mainly deviations are observed for (C1-H7), (C2-H8),(C15-H22), (C5-H11), (N25-H26), and (N28-H31) bond lengths. These values are respectively observed at 1.08316 Å, 1.08401 Å, 1.08182 Å, 1.08319 Å, 1.01427 Å, and 1.05149 Å.The corresponding experimental values for these bond lengths are 0.93026 Å, 0.93024 Å, 0.92956 Å, 0.93014 Å, 0.86040 Å, and 0.86024 Å respectively. It can be noted easily that calculated values are in characteristic range of C-H and N-H bond lengths while experimental values have relatively lower values. This may be very well explained in terms of intermolecular hydrogen bonding

Table 1. Optimized geometrical parameters (bond lengths, bond angles, Torsion angles) of MBZ calculated by DFT and compared with XRD data.

Bond Lengths			Bond Angles		
Geometrical parameters	Experimental values (Å) [Eduardo L. Gutierrez et al.[9]]	Optimized Values (Å) B3LYP/6-311++G(d,p)	Geometrical parameters	Experimental values (°) [Eduardo L. Gutierrez et al.[9]]	Optimized values (°) B3LYP/6-311++G(d,p)
v(C1-H7)	0.93026	1.08316	H1-C1-C6	120.1033	118.72054
C1-C2	1.37112	1.38933	H7-C1-C2	120.01327	120.88999
C1-C6	1.38787	1.40233	H8-C2-C3	119.54637	120.04953
C2-H8	0.93024	1.08401	H9-C3-C4	120.14888	119.95974
C2-C3	1.37201	1.39608	H10-C4-C5	120.00521	119.78985
C3-C4	1.36735	1.39332	H11-C5-C6	119.85003	120.22929
C4-C5	1.38609	1.39308	C1-C2-C3	120.85003	120.03998
C5-C6	1.37796	1.40136	C2-C3-C4	119.69443	120.00001
C5-H11	0.93014	1.08319	C3-C4-C5	120.02177	120.06001
C4-H10	0.92999	1.08384	C4-C5-C6	120.37836	120.28001
C3-H9	0.93000	1.08417	C6-C1-C2	119.88140	120.38946
C6-C12	1.49700	1.49720	H22-C15-C14	121.36022	121.84002
C12-C14	1.49247	1.50512	C15-C14-C12	121.02888	122.02998
C14-C15	1.38682	1.39869	C14-C12-C6	118.51930	120.31001
C15-H22	0.92956	1.08182	C6-C12-013	120.31622	120.38005
C5-H11	0.93014	1.08319	C14-C12-013	121.15365	119.30850
C12-O13	1.21360	1.21993	H22-C15-C16	121.36112	120.81131
C14-C19	1.40519	1.41127	C12-C14-C19	118.64263	117.22712
C19-C18	1.37603	1.38776	C14-C19-H20	118.76972	117.81284
C18-C17	1.38913	1.39151	C18-C19-H20	118.71371	120.10997
C17-C16	1.38649	1.40412	H21-C18-C17	121.89332	121.82000
C15-C16	1.34479	1.38955	C17-C16-C15	122.06638	121.45998
C19-H20	0.92961	1.08241	C15-C14-C19	120.26694	120.61421
C18-H21	0.92940	1.08295	C16-C15-C14	117.27866	117.33000
C17-N25	1.38773	1.39399	C14-C19-C18	122.51656	122.07511
C16-N23	1.38872	1.39424	C19-C18-C17	116.28025	116.77998
N23-C24	1.32880	1.33305	N23-C16-C17	106.52424	107.42997
N25-C24	1.33344	1.35225	C16-C17-N25	106.62435	105.96249
N25-H26	0.86040	1.01427	C17-N25-C24	108.43251	108.29686
N23-H27	0.85952	1.09962	N25-C24-N23	109.82893	110.40001
C24-N28	1.34859	1.35393	C24-N23-H27	125.75008	123.28362
N28-H31	0.86024	1.05149	C16-N23-H27	125.66362	128.72994
N28-C29	1.37917	1.38431	H26-N25-C17	125.80996	130.38297
C29-O30	1.19726	1.21717	H26-N25-C24	125.75753	121.31998
C29-O32	1.32633	1.32805	N23-C24-N28	122.91133	123.19000
C33-032	1.44937	1.44428	C24-N28-C29	123.31775	122.48999
C33-H34	0.96043	1.08996	C29-N28-H31	118.30194	122.14937
C33-H35	0.95972	1.08655	N28-C29-O30	124.04512	124.18004
C33-H36	0.96037	1.08996	N28-C29-O32	108.93171	110.04001
N40-O39	1.23322	1.21523	O30-C29-O32	127.02178	125.77995
N40-O38	1.24110	1.26986	C29-O32-C33	115.95689	116.26005
N40-037	1.24243	1.28776	O32-C33-H34	109.55400	110.19999
		O32-C33-H35	109.46731	104.88001	
		O32-C33-H36	109.54865	110.18704	
		H36-C33-H35	109.44152	110.80216	
		H34-C33-H36	104.39189	109.85329	
		H35-C33-H34	109.42381	110.82104	
		O37-N40-O38	120.23502	118.41601	
		O38-N40-O39	119.53415	121.49212	
		O39-N40-O37	120.09179	120.09179	

Torsion angles					
Geometrical parameters	Experimental values (°)	Optimized values (°)	Geometrical parameters	Experimental values (°)	Optimized values (°)
H9-C3-C4-C5	-178.12210	-179.20104	N23-C16-C17-N25	-0.00681	0.19224
H10-C4-C5-C6	177.80850	179.28967	N25-C17-C18-H21	172.54993	0.23452
H11-C5-C6-C1	-179.22937	177.96748	H21-C18-C19-H20	-8.64404	-1.12844
H7-C1-C2-C3	179.94236	178.74060	C14-C15-C16-C17	19.98623	-0.49462
H8-C2-C3-C4	179.82575	179.82575	C15-C16-C17-C18	-1.52114	0.58652
H10-C4-C5-H11	-2.24669	0.94824	C16-C17-C18-C19	-1.30957	0.17202
H11-C5-C6-C12	0.27366	1.53157	C17-C18-C19-C14	19.69132	-1.00622
C12-C6-C1-H7	1.36242	-1.99686	C18-C19-C14-C15	179.78150	1.11316
H7-C1-C2-H8	-0.97482	-0.99563	C19-C14-C15-C16	-0.32699	-0.32533
H8-C2-C3-H9	-0.37611	0.01178	C15-C16-N23-C24	179.79721	179.71721
H9-C3-C4-H10	1.92032	0.66439	C16-N23-C24-N28	179.71721	-179.64942
C1-C2-C3-C4	-0.39220	0.08987	C16-C17-N25-H26	-179.64942	-179.89593
C2-C3-C4-C5	1.97680	0.98484	C18-C17-N25-H26	-0.6578	-0.32699
C3-C4-C5-C6	-2.14907	-0.84442	C17-N25-C24-N28	1.92032	179.76676
C4-C5-C6-C1	0.71540	-0.36128	N23-C24-N25-H26	-0.39220	179.74824
C5-C6-C1-C2	0.86358	1.43877	N23-C24-N25-H17	1.97680	-0.10796
C6-C1-C2-C3	-1.03886	-1.30838	C24-N25-C17-C16	-2.14907	-0.05707
C1-C6-C12-O13	-54.69063	-29.02453	N28-C24-N25-H26	0.71540	-0.375692
C6-C12-C14-C19	172.54993	154.16734	N23-C24-N28-H31	0.86358	-1.550172
O13-C12-C14-C19	-8.64404	-26.26654	C24-N28-C29-O32	-1.03886	179.51220
H20-C19-C14-C15	179.98623	-178.35382	C24-N28-C29-O30	-54.69063	-0.50111
C12-C14-C15-C16	-177.52114	-176.10248	N25-C24-N28-C29	-0.32699	0.21056
H22-C15-C16-C17	-179.30957	-178.95296	N28-C29-O32-C33	179.76676	-179.81975
N23-C16-C17-C18	179.69132	-179.43299	O30-C29-O32-C33	179.74824	0.19383
N25-C17-C18-C19	179.78150	-179.34072	H31-N28-C9-O30	-0.10796	-178.77122
H21-C18-C19-C14	-179.85596	179.41660	H31-N28-C9-O32	-0.05707	1.24209
H20-C19-C14-C12	-2.83730	-178.35382	C29-O32-C33-H36	54.9976	60.72873
C12-C14-C15-H22	2.48380	2.33890	C29-O32-C33-H34	-58.4762	-60.65970
H22-C15-C16-N23	0.32879	1.07174	C29-O32-C33-H35	-170.6541	-179.97770

Table 2. Vibrational wavenumbers, IR intensities and Raman scattering activities of the MBZ-N molecule along with % Potential Energy distribution.

Mode	Unscaled wavenumbers (cm ⁻¹)	Scaled wavenumbers (cm ⁻¹)	CALCULATED		EXP wavenumbers [9] (cm ⁻¹)		Assignment (%PED of internal coordinates) having contribution >10% are shown
			IR Intensity	RAMAN Activity	IR	RAMAN	
1	3562.57	3227.69	256.7202	134.6907	3208		v(N25H26)(92)
2	3210.29	3069.04	0.6127	72.0765	3068	3065	v(C15H22)(98)
3	3208.35	3067.18	3.0385	135.5361	3068	3065	v(C19H20)(82)+v(C18H21)(16)
4	3199.03	3058.27	7.6428	236.7985	3068	3065	v(C1H7)(70)+v(C2H8)(17)
5	3193.7	3053.18	8.3254	112.5258	3052	3058	v(C5H11)(36)+ v(C4H10)(36)+v(C1H7)(13)+ v(C3H9)(13)
6	3191.6	3051.17	1.3028	81.0564	3052	3058	v(C18H21)(82)+v(C19H20)(17)
7	3185.09	3044.95	17.1975	74.9809	3052	3058	v(C3H9)(37)+ v(C5H11)(36)+v(C2H8)(17)
8	3176.79	3037.01	4.0041	135.384	3052	3058	v(C2H8)(37)+ v(C4H10)(36)+v(C5H11)(21)
9	3174.06	3034.40	7.9333	86.6706	3052	3058	v(C33H35)(81)
10	3167.23	3027.87	0.5025	42.9106	3052	3058	v(C3H9)(43)+v(C2H8)(27)+v(C4H10)(23)
11	3137.89	2999.82	13.6819	54.2984			v(C33H34)(50)+v(C33H36)(50)
12	3059.9	2925.26	31.6738	207.5718	2960	2959	v(C33H36)(41)+v(C33H34)(40)+v(C33H35)(17)
13	2931.16	2916.86	2004.3627	241.1328	2882		v(N28H31)(54)+v(H31O38)(44)
14	2175.48	2164.86	2730.7154	103.6781	2132		v(N23H27)(54)+v(H27O37)(41)
15	1763.79	1755.18	288.9271	133.0242			δ (C24C29N28)(47)+ δ (C29N28O38)(20)
16	1717.46	1709.08	563.7464	181.2957			δ (C24N28O38)(33)+ δ (C24N23O37)(23)+ v(C24C29)(21)+ δ (C16N23O37)(12)
17	1713.78	1705.42	170.906	118.6965	1759		δ (C24N28O38)(42)+v(C24N28)(19)+ δ (C 24N23O37)(11)
18	1690.03	1681.78	453.1316	190.326			δ (C24N28O38)(43)+ δ (C29N28O38)(18)
19	1637.49	1629.50	114.7411	119.4074			δ (C24N28O38)(32)+ δ (C29N28O38)(17)
20	1636.4	1628.41	34.9019	51.2675			δ (C24N28O38)(28)+ δ (C29N28O38)(20)
21	1622.54	1614.62	7.3869	275.9037			δ (C16N23O37)(23)+ δ (C29N28O38)(17)
22	1615.6	1607.72	6.0175	22.4474			v(C3C4)(15)+v(C2C3)(13)
23	1557.03	1549.43	196.0609	114.0093	1564	1572	v(C24N28)(29)+v(C24N28)(25)+ δ (C16N 25C17)(13)
24	1531.94	1524.46	783.8508	12.2017			δ (C24N28O38)(27)+ δ (C16N23O37)(14)+ v(O39N40)(11)
25	1519.68	1512.26	3.0688	3.2176			δ (C1H8C2)(16)+ δ (C3H10C4)(15)+ δ (C4H 11C5)(14)+ δ (C6H7C1)(14)
26	1498.08	1490.77	26.9311	19.2269	1498		v(C17N25)(15)+ δ (C24N28)(13)+ δ (N23C 17C16)(12)+ δ (C24N28O38)(12)
27	1497.19	1489.88	3.8619	7.0192			δ (C29N28O38)(27)+ δ (H35H36C33)(18)+ δ (C24C29N28)(18)
28	1486.46	1479.21	11.3608	15.0161			δ (H34H35C23)(70)+ δ (H35H36C33)(22)
29	1480.06	1472.84	156.9506	8.8574			δ (C29N28O38)(42)+v(N28C29)(16)+ δ (C 24C29N28)(15)

30	1475.97	1468.77	19.6844	2.4503			$\delta(C4H9C3)(24)+\delta(C5H10C4)(14)+v(C4C5)(12)+\delta(C1H8C2)(12)$
31	1457.95	1450.84	80.3619	50.0055	1386	1370	$\delta(C24C29N28)(29)+\delta(C29N28O38)(20)+v(C24N28)(13)$
32	1450.27	1443.19	66.6247	44.7062			$\delta(C29N28O38)(23)+\delta(C24C29N28)(16)$
33	1391.44	1384.65	23.7943	74.7062			$v(C24N28)(20)+\delta(C24N28O38)(18)+\delta(C16N23O37)(16)$
34	1352.03	1345.43	8.5321	1.0407	1281	1298	$\delta(C2H7C1)(22)+\delta(C6H11C5)(21)+v(C1C2)(11)$
35	1335.78	1329.26	31.4483	110.0716			$\delta(C29N28O38)(36)+\delta(C24N28O38)(15)$
36	1329.6	1323.11	7.2735	128.3833		1251	$\delta(C29N28O38)(29)+\delta(C24N28O38)(28)+v(C24N28)(14)$
37	1318.37	1311.94	63.52	97.726			$\delta(C29N28O38)(33)+\delta(C16N23O37)(24)+v(N28C29)(11)$
38	1301.8	1295.45	1841.111	32.6641	1244	1215	$\delta(C29N28O38)(64)+v(N28C29)(21)$
39	1268.68	1262.49	166.5773	10.1921			$\delta(C24N28O38)(30)+\delta(N23C17C16)(17)+v(H31O38)(11)$
40	1250.56	1244.46	97.7398	9.2412			$\delta(C29N28O38)(36)+v(H31O38)(25)$
41	1233.07	1227.05	27.6037	141.5339	1203	1215	$\delta(C24N23O37)(22)+\delta(C29N28O38)(20)+\delta(C16N23O37)(24)$
42	1221.07	1215.11	18.2781	13.8701	1203	1215	$\delta(C29N28O38)(30)+\delta(C24N28O38)(27)+v(C24N28)(17)$
43	1212.23	1206.31	8.651	19.0376			$v(H31O38)(22)$
44	1200.5	1194.64	33.3632	3.4142			$\delta(C16N23O37)(14)+\delta(C6H11C5)(13)+\delta(C5H10C4)(12)+\delta(C2H7C1)(12)$
45	1185.06	1179.28	0.2485	5.0414	1132	1156	$\delta(C4H9C3)(36)+\delta(C1H8C2)(21)+\delta(C5H10C4)(16)$
46	1174.18	1168.45	0.5513	3.0839			$\delta(H34O32C33)(66)+\delta(H35O32C33)(23)$
47	1154.36	1148.73	7.9633	9.6007			$\delta(C29N28O38)(12)+\delta(C24N23O37)(12)$
48	1137.26	1131.71	4.9633	39.304			$\delta(C29N28O38)(26)+\delta(C24N28O38)(22)+\delta(C24N23O37)(16)+\delta(C16N23O37)(12)$
49	1105.91	1100.51	24.6583	1.3476			$\delta(C29N28O38)(40)+\delta(C24N28O38)(22)$
50	1102.73	1097.35	82.6087	9.9141			$\delta(C29N28O38)(33)+\delta(C24N28O38)(19)$
51	1097.48	1092.12	122.6764	5.9755			$\delta(C29N28O38)(41)+\delta(C24N28O38)(17)+v(H31O38)(13)$
52	1061.57	1056.39	153.2189	31.64			$v(H31O38)(43)+\delta(C16N23O37)(17)+\delta(C29N28O38)(13)+v(H27O37)(12)$
53	1048.68	1043.56	3.9113	32.0975			$v(C2H3)(24)+v(C3C4)(23)$
54	1028.4	1023.38	128.1559	54.5142			$\delta(C24C29N28)(33)+v(H31O38)(12)$
55	1016.22	1011.26	2.8388	47.9342			$\delta(C6C2C1)(50)$
56	1012.51	1007.57	0.4085	0.1817			$\Upsilon(H9C2C4C3)(28)+\Upsilon(H8C1C3C2)(24)+\Upsilon(H10C3C5C4)(16)+\delta(C5C1C6)(15)$
57	996.34	991.48	2.152	0.0315			$\Upsilon(H11C6C4C5)(26)+\Upsilon(H7C6C2C1)(24)+\Upsilon(H11C6C4C5)(21)+\Upsilon(H8C1C3C2)(16)$
58	981.72	976.93	32.3208	18.5757			$\delta(C24C29N28)(64)+v(H31O38)(16)$
59	975.8	971.04	3.6626	0.0958			$\delta(C24C29N28)(48)+\Upsilon(H20C14C18C19)(13)+v(H31O38)(12)$
60	962.79	958.09	5.6627	9.481			$\delta(C24C29N28)(54)+v(H31O38)(17)+\delta(C24N28O38)(14)$
61	950.18	945.54	9.3599	1.8768	967	953	$\delta(C24C29N28)(25)+\delta(C24N28O38)(17)$

62	921.37	916.87	8.7038	1.1053			$\Upsilon(H31C24C29N28)(31)+\tau(N23C24N28C29)(29)+\tau(C16N23N40O39)(11)$
63	915.92	911.45	45.4735	0.1555			$\Upsilon(H31C24C29N28)(51)+\tau(N23C24N28C29)(48)$
64	900	895.61	100.4348	16.5763	896		$v(H27O37)(17)+\delta(C24N23O37)(16)+\delta(C16N23O37)(14)+\delta(N23C17C16)(13)$
65	866.61	862.38	41.8544	13.8884			$\delta(C16N23O37)(18)+\delta(C24C29N28)(16)+v(H31O38)(12)+v(H27O37)(11)+\delta(C24N23O37)(11)$
66	862.36	858.15	5.392	3.6136			$\Upsilon(H8C1C3C2)(16)+\Upsilon(H7C6C2C1)(15)+\Upsilon(H11C6C4C5)(15)+\Upsilon(H10C3C5C4)(14)$
67	843.57	839.45	12.9167	0.9443	842	864	$\tau(N25C24N23C16)(23)+\tau(N25C24N23C16)(22)+\Upsilon(H21C19C17C18)(18)$
68	807.96	804.02	18.8545	0.1367			$\tau(C16N23N40O39)(65)+\tau(N28O38N40O39)(22)+\tau(N40O38N28C29)(13)$
69	805.83	801.90	21.6542	4.689	789	792	$\tau(C16N23N40O39)(32)+\tau(N25C24N23C16)(14)$
70	777.2	773.41	36.3577	0.2138			$\tau(N40O38N28C29)(48)+\Upsilon(H31C24C29N28)(35)$
71	761.77	758.05	12.9722	5.3439			$\delta(C24C29N28)(42)+v(H31O38)(22)+\tau(N25C24N23C16)(13)$
72	758.7	755.00	38.363	2.802	748		$\delta(C24C29N28)(42)+v(H31O38)(23)+\tau(N25C24N23C16)(11)$
73	742.87	739.24	80.0765	3.1345			$\delta(C24N28O38)(27)+\delta(C29N28O38)(23)+v(H27O37)$
74	739.44	735.83	1.1914	1.8686			$\delta(C29N28O38)(50)+v(H31O38)(18)$
75	730.31	726.75	64.7963	3.3808	724	756	$\tau(N25C24N23C16)(34)+\tau(C16N23N40O39)(32)$
76	721.82	718.30	11.4386	16.9291			$\delta(C24C29N28)(37)+\delta(C24N28O38)(20)+\delta(N23C17C16)(13)$
77	716.12	712.63	9.8716	0.5837			$\tau(N25C24N23C16)(61)+\Upsilon(N28N23N25C24)(21)$
78	712.62	709.14	12.6678	2.1626			$\delta(C24N28O38)(46)+\delta(C24N23O37)(14)+v(H31O38)(11)$
79	706.01	702.56	28.4768	0.4726			$\delta(C5C1C6)(21)+\delta(C24C29N28)(20)+\delta(N23C17C16)(16)$
80	673.31	670.02	60.0215	2.393			$\delta(N23C17C16)(39)+v(H27O37)(13)$
81	663.75	660.51	51.5946	0.6748			$\tau(N25C24N23C16)(45)+\tau(N25C24N23C16)(17)$
82	632.22	629.13	0.262	5.5119			$\delta(C6C2C1)(50)+\delta(C1C3C2)(16)$
83	604.63	601.68	20.9935	6.8969			$\tau(N25C24N23C16)(28)+\tau(C16N23N40O39)(27)$
84	590.54	587.66	22.6461	2.2435	576		$\delta(C29N28O38)(52)+\delta(C24C29N28)(11)$
85	541.83	539.19	0.9837	5.1069	523		$\tau(C16N23N40O39)(23)+\tau(N25C24N23C16)(22)+\delta(C24N23O37)(11)+\delta(C16N23O37)(11)$
86	513.66	511.15	8.5493	0.7409	494		$\delta(C16N23O37)(39)+\delta(C24N23O37)(23)+\delta(C24N28O38)(19)$
87	441.9	439.74	1.5807	0.5066	429		$\delta(C24C29N28)(29)+\delta(C29N28O38)(28)$
88	438.09	435.95	1.8841	2.329			$\tau(C16N23N40O39)(58)+\tau(N25C24N23C16)(16)$
89	413.93	411.91	0.6158	1.4149			$\tau(C16N23N40O39)(39)+\delta(C6C1C2C3)$
90	397.17	395.23	1.0765	2.5569			$\delta(C29N28O38)(33)+v(H31O38)(19)$
91	377.17	375.33	7.2778	1.7309			$\delta(C24C29N28)(48)+v(H31O38)(30)$

92	354.43	352.70	8.0443	0.88			$\tau(C16N23N40O39)(38)+\tau(N25C24N23C16)(19)+\gamma(H31C24C29N28)(16)$
93	312.74	311.21	7.277	2.8381			$\delta(C24C29N28)(29)+\tau(C16N23N40O39)(23)+\delta(C29N28O38)(22)$
94	297.81	296.36	43.6606	2.5591			$\delta(C24N28O38)(48)+\nu(H27O37)(19)+\delta(C24N23O37)(12)$
95	286.96	285.56	0.3603	1.8073			$\tau(C16N23N40O39)(59)+\tau(N23C24N28C29)(22)$
96	237.55	236.39	13.7804	1.2872			$\nu(H31O38)(52)+\delta(C29N28O38)(23)+\nu(H27O37)(13)$
97	224.03	222.94	82.0732	0.7598			$\nu(H31O38)(38)+\nu(H27O37)(30)+\delta(C29N28O38)(11)$
98	217.21	216.15	8.3516	0.9211			$\gamma(H31C24C29N28)(20)+\tau(N28O38N40O39)(19)+\nu(H31O38)(18)+\tau(C16N23N40O39)(16)+\tau(N40O38N28C29)(15)$
99	197.51	196.55	3.3108	1.5405			$\tau(N40O38N28C29)(22)+\gamma(H31C24C29N28)+\nu(H31O38)(16)+\tau(N23C24N28C29)(15)+\tau(N28O38N40O39)(11)$
100	179.13	178.26	0.9199	2.4031			$\nu(H31O38)(58)$
101	169.33	168.50	3.0641	0.4283			$\delta(C24N28O38)(52)+\nu(H31O38)(31)$
102	148.15	147.43	1.1825	0.7824			$\tau(C16N23N40O39)(39)+\tau(N25C24N23C16)(24)+\tau(N40O38N28C29)(12)$
103	123.08	122.48	0.5681	1.0086			$\tau(N23C24N28C29)(34)+\tau(N40O38N28C29)(22)+\gamma(H31C24C29N28)(19)+\tau(N28O38N40O39)(19)$
104	108.95	108.42	2.753	2.3035			$\tau(C16N23N40O39)(76)$
105	90.28	89.84	1.3634	1.4106			$\tau(C16N23N40O39)(29)+\delta(C29N28O38)(28)+\tau(N23C24N28C29)(19)+\delta(C24C29N28)(11)$
106	84.62	84.21	1.3915	3.4779			$\tau(N28O38N40O39)(54)+\tau(C16N23N40O39)(42)$
107	82.3	81.90	3.2757	1.2199			$\tau(C16N23N40O39)(44)+\tau(N28O38N40O39)(43)$
108	63.92	63.61	1.2808	2.5896			$\delta(C29N28O38)(46)+\nu(H31O38)$
109	50.45	50.20	1.3024	2.2716			$\tau(N28O38N40O39)(46)+\tau(C16N23N40O39)(22)+\delta(C29N28O38)(11)$
110	47.66	47.43	1.6516	0.5778			$\tau(N28O38N40O39)(54)+\tau(C16N23N40O39)(17)$
111	33.85	33.68	3.4423	3.3966			$\tau(N28O38N40O39)(49)+\tau(N40O38N28C29)(14)+\delta(C29N28O38)(11)$
112	29.55	29.41	1.2888	1.4574			$\tau(N40O38N28C29)(49)+\tau(N28O38N40O39)(44)$
113	21.84	21.73	0.4576	1.0986			$\tau(N28O38N40O39)(55)+\tau(N40O38N28C29)(40)$
114	18.28	18.19	3.185	0.982			$\tau(N40O38N28C29)(56)+\tau(N28O38N40O39)(29)$

Some vibrations which are used in the table can be defined as: ν stretching ; δ deformation (bending) ; τ torsion ; γ out-of-plane bending.

in unit cell. Similarly, dihedral angles affected by these interactions show deviations between theoretical and experimental values. From the Table 1, it is visible that mainly dihedral angles (C1-C6-C12-O13) and (C24-N28-C29-O30) show significant deviations of 25.66° and 54.19° respectively. Figure 1 depicts that these dihedral angles are across single bonds and easily vulnerable for twisting due to presence of oxygen atom which can form inter-molecular hydrogen bonding. Despite of these minor deviations from experimental structure, optimized structure can be used for further analysis with satisfactory accuracy in the calculated properties.

3.2. Vibrational spectra

Infrared spectroscopy is a technique based on the vibrations of the atoms of a molecule. Infrared spectroscopy has proved to be a powerful tool for the study of biological molecules and the application of this technique to biological problems is continually expanding, particularly with the advent of increasingly sophisticated sampling techniques such as infrared imaging. Biological systems, including lipids, proteins, peptides, biomembranes, nucleic acids, animal tissues, microbial cells, plants and clinical samples, have all been successfully studied by using infrared spectroscopy [14]. Raman spectroscopy has emerged as one of the most often used spectroscopic methods for the identification of large biological molecules and other species such as bacteria. In last few years several studies of the application of Raman spectroscopy for biological molecules have been reported [15-18].

The MBZ-N has 40 atoms that provide 114 (3N-6) vibrational modes. The vibrational assignments, experimental frequencies and calculated vibrational wavenumbers, IR intensities and Raman scattering activities of the MBZ-N have been listed in Table 2. The harmonic vibrational wavenumbers computed by B3LYP/6-311++G(d,p) level are higher due to missing anharmonicity terms. Therefore, computed harmonic vibrational wavenumbers have been scaled down with three different scaling factors, wavenumbers $\geq 3250 \text{ cm}^{-1}$ (0.906), 3000-3250 cm^{-1} (0.956) and below 3000 cm^{-1} (0.99512) as suggested in literature by Anju Maurya et al.[19]. The scaled and experimental FTIR and Raman spectra have been compared in Figure 2 and Figure 3 respectively.

It can be seen that an excellent matching is obtained between the two. The N-H stretching gives absorption bands at higher frequency (above 3200 cm^{-1}) region of the vibrational spectrum without intra- and inter-molecular hydrogen bond interactions. However, they shift towards red region under the effect of these interactions. The observed peak at 3208 cm^{-1} in IR spectrum has been assigned to stretching mode of the N25-H26 and calculated at 3208 cm^{-1} . The amide mode (N23-H27) calculated at 2165 cm^{-1} is assigned to a shoulder at 2132 cm^{-1} in IR spectrum. The CH stretching wavenumbers calculated by DFT, can be assigned to

broad band at 3068 cm^{-1} in FT-IR spectrum and a sharp peak at 3065 cm^{-1} in Raman spectrum with more than 90% contribution in PED. The C-N stretching bands appear at 1564 cm^{-1} (stretching mode of C24N28) and 1498 cm^{-1} (stretching mode of C17-N25) in FTIR and a weak band at 1572 cm^{-1} in Raman spectrum.

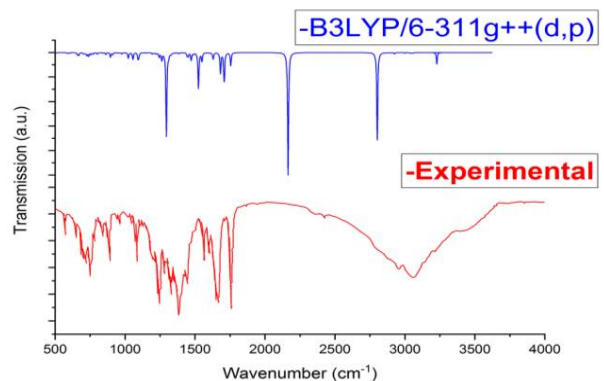


Figure 2. Computational and experimental[9] FTIR spectra of MBZ-N.

3.3. Natural Bond Orbital (NBO) analysis

NBO analysis was performed by the NBO 5.0 program implemented in Gaussian 09 package at B3LYP/6-311++G(d,p) level of theory. Natural bond orbital analysis is an efficient method for understanding intra- and inter-molecular bonding and interaction among bonds. It can also investigate charge transfer or conjugative interaction in molecular systems. The second-order Fock matrix was formed to evaluate the donor-acceptor interactions in the NBO analysis [20]. The interactions result in a loss of occupancy from the localized NBO of the idealized Lewis structure into an empty non-Lewis orbital. For each donor (i) and acceptor (j), the stabilization energy E(2) associated with the electron delocalization $i \rightarrow j$ is estimated as—

$$E(2) = -n_s[\langle s|F|s\rangle^2/(e_{s^*} - e_s)] = -n_\sigma \left[\frac{F_{ij}^2}{\Delta E} \right];$$

Here $s|\langle s|F|s\rangle^2$ or F_{ij}^2 is the Fock matrix element which corresponds to i and j NBO orbitals. n_s is the population of the donor s orbital, e_{s^*} and e_s are the energies of s^* and s NBOs.

The larger the E(2) value, the more intensive is the interaction between electron donors and electron acceptors, i.e. the more donating tendency from electron donors to electron acceptors and the greater the extent of conjugation of the whole system. The intra-molecular interaction are formed by the orbital overlap between $\sigma(\text{C}-\text{C})$ and $\sigma^*(\text{C}-\text{C})$ and $\pi(\text{C}-\text{C})$ and $\pi^*(\text{C}-\text{C})$ bond orbital which results intra-molecular charge transfer (ICT) causing stabilization of the molecular system. The results of second-order perturbation theory analysis of

Table 3. Second order perturbation theory analysis of Fock matrix in NBO basis

Donor NBO(i)	ED(i)/e	Acceptor NBO(j)	ED(j)/e	$E^{(2)a}$ kcal mol ⁻¹	$E(j)-E(i)^b$ (a.u.)	$F(i,j)^c$ (a.u.)
π C 1 - C 2	1.65112	π^* C 3 - C4 π^* C 5 - C6	0.31567 0.37194	21.37 19.56	0.28 0.28	0.070 0.066
π C 3 - C 4	1.645411	π^* C 1 - C2 π^* C 5 - C6	0.28930 0.37194	18.10 22.12	0.29 0.28	0.065 0.071
π C 5 - C 6	1.64636	π^* C 1 - C2 π^* C 3 - C4 π^* C12-O 13	0.28930 0.31567 0.15970	19.43 18.51 14.64	0.29 0.29 0.27	0.068 0.066 0.059
σ C 14 -C 15	1.96959	σ^* C16 - N 23	0.02455	5.93	1.12	0.073
π C 14 -C 15	1.66936	π^* C 12-O 13 π^* C 16 -C17 π^* C18- C 19	0.15970 0.46166 0.29198	14.05 19.19 19.66	0.29 0.29 0.29	0.059 0.069 0.067
π C 16 - C 17	1.61400	π^* C 14- C 15 π^* C 18 - C19 π^* N23- C 24	0.34902 0.29198 0.52682	14.46 16.19 11.31	0.40 0.31 0.21	0.068 0.064 0.045
σ C16 -N 23	1.97998	σ^* C 24 -N 28	0.02266	5.28	1.25	0.073
σ C18 - C 19	1.97196	σ^* C 17 -N 25	0.02682	6.15	1.24	0.078
π C18 - C 19	1.69433	π^* C 14- C 15 π^* C 16- C 17	0.34902 0.46166	13.37 20.68	0.38 0.29	0.064 0.072
π N23 - C 24	1.89874	π^* C 16-C 17	0.46166	14.94	0.40	0.076
σ N28 -H 31	1.97402	σ^* C24 -N 25	0.02538	6.59	1.10	0.076
n2 (O 13)	1.88778	σ^* C 6 - C 12 σ^* C 12 - C14	0.06381 0.06628	18.49 19.40	0.70 0.68	0.103 0.104
n1 (N 25)	1.60162	π^* C16 -C 17 π^* N23 -C24	0.46166 0.52682	29.35 73.71	0.33 0.23	0.089 0.120
n1 (N 28)	1.63661	π^* N 23 -C24 π^* C29 -O 30	0.52682 0.35208	74.59 52.26	0.22 0.30	0.119 0.113
n2 (O 30)	1.84386	σ^* N28 -C 29 σ^* C29 -O 32	0.07396 0.08537	22.98 28.08	0.69 0.66	0.115 0.124
n1 (O 32)	1.95900	σ^* C29 -O30	0.02324	8.93	1.15	0.091
n2(O 32)	1.79204	π^* C29 -O30	0.35208	45.92	0.36	0.119
π^* C12 -O13	0.15970	π^* C 5 - C 6 π^* C 14 - C 15	0.37194 0.34902	102.48 14.65	0.01 0.09	0.062 0.064
π^* C14 - C 15	0.34902	σ^* C 17 - N25	0.02682	6.71	0.41	0.108
π^* C 16 - C 17	0.466166	π^* C14 - C 15 σ^* C33- H36	0.34902	45.36 6.59	0.09 3.28	0.089 0.270
π^* C 18 - C19	0.291980	π^* C14 - C 15	0.34902	29.05	0.09	0.082
π^* N 23 - C24	0.52682	π^* C16 - C 17	0.46166	13.92	0.09	0.046
π^* C 29 - O 30	0.35208	π^* C14 - C 15 σ^* O39 -N40	0.34902 0.63586	15.30 24.92	0.10 2.93	0.059 0.343
π^* C 14 - C 15	0.34902	σ^* O39 - N40	0.63586	59.89	2.83	0.524
σ O37 - N40	1.99436	σ^* C33 - H36 σ^* O39-N 40	0.01193 0.63586	20.86 7.21	4.26 3.90	0.266 0.181
σ O38 - N40	1.99539	σ^* C33- H36	0.01193	27.85	4.28	0.309
π O39 - N40	1.99593	σ^* C 17- N25	0.02682	5.56	1.58	0.084
n1 (O 37)	1.96646	σ^* N23 - H27 σ^* O39 -N40	0.14063 0.63586	8.45 9.72	0.97 3.58	0.083 0.199
n2 (O 37)	1.83125	σ^* N23 -H27 σ^* C33 - H36 π^* O39 -N40	0.14063 0.01193 0.63586	64.70 12.14 13.87	0.74 3.71 0.89	0.197 0.197 0.102
n1 (O 38)	1.96368	σ^* N28 - H31 σ^* C33 - H36 σ^* O37- N40 σ^* O37- N40 σ^* O 39- N40	0.07773 0.01193 0.09708 0.09708 0.63586	8.13 8.79 7.23 6.06 6.45	1.06 3.99 2.42 1.03 3.63	0.084 0.168 0.234 0.072 0.163
n2 (O38)	1.88113	σ^* N28 -H 31 σ^* C33 - H 36 σ^* O37 - N40 σ^* O39 - N40 π^* O39 - N40	0.07773 0.01193 0.09708 0.63586 0.63586	28.03 8.70 9.18 6.24 18.52	0.72 3.65 0.69 3.30 0.83	0.129 0.164 0.072 0.149 0.113
n2 (O39)	1.88044	σ^* C33 - H 36	0.01193	16.90	3.55	0.225

σ O 39 - N40	1.99673	σ^* O38 - N40	0.08693	6.75	2.83	0.126
π O39 - N 40	1.99593	σ^* O39 - N40	0.63586	34.35	4.00	0.400
n3 (O 38)	1.65010	σ^* O39 -N40	0.63586	6.37	3.20	0.138
n1 (O 39)	1.98134	σ^* O39 -N40	0.63586	16.81	3.71	0.268
n2 (O 39)	1.88044	σ^* O37 - N40	0.09708	25.35	0.59	0.109
		σ^* O38 -N40	0.08693	5.99	2.66	0.114

Fock Matrix in NBO of the MBZ-N have been listed in Table 3. The intra-molecular conjugative interaction of the π (C1-C2) with antibonding orbital of π^* (C3-C4) and π^* (C5-C6) leads to a strong delocalization with conjugation energy of 21.37 kcal/mol and 19.56 kcal/mol respectively. Other conjugative interactions among the various π and π^* bonds of aromatic rings have similar interaction energy range. The large electron delocalization, related to the resonance in the molecule, is observed for electron donating interaction from the n1(N25), n1(N28),n2(O37) and n2(O39) to nearest π^* bonds with interaction energy of 73.71, 74.59, 64.70 and 25.35 kcal/mol respectively. The highest interaction energy of 102.48 kcal/mol is observed for electron delocalization from $\pi^*(C12-O13)$ to $\pi^*(C5-C6)$ anti-bonding orbitals. This electron delocalization is responsible for generation of electron rich and electron deficient sites in the molecule which are responsible for biological activities.

3.4. Molecular electrostatic potential(mep) surface analysis

MEP is a very important tool to visualize possible hydrogen bonding, chemical reactivity, inter- and intra-molecular interactions of a molecule. It is used to locate the reactive sites inside the compounds [21]. The positive electrostatic potential regions are nucleophilic and the negative electrostatic potential regions are the electrophilic sites in a molecule. They are respectively represented by blue and red colour within the MEP profile. The MEP surface for title molecule has been computed at the mentioned computational level to define the nucleophilic and electrophilic sites, as shown in Figure 4. In the MEP surface, negative regions are localized on oxygen atoms and the values of negative electrostatic potential for O38 and O39 are -0.039005 a.u. and -0.0551154 a.u. respectively. Similarly the positive regions are spread over nitrogen atoms. The dispersion of charges in given molecule is in the range of -0.07049 a.u. to 0.07049 a.u.

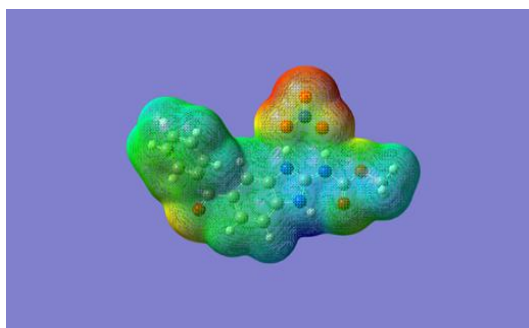


Figure 4. Molecular Electrostatic Potential mapped on the isodensity surface for MBZ calculated at the B3LYP/6-311++G(d,p) level of theory.

3.5. HOMO- LUMO Analysis

Highest occupied molecular orbitals (HOMO) and lowest unoccupied molecular orbitals (LUMO) are frontier orbitals which are widely used to describe different characteristic features of the molecules. The knowledge about these FMO (frontier molecule orbitals) is used to determine electronic transitions, charge transfers and several molecular electronic features of any molecular system. A molecule having a small frontier orbital gap is more polarizable and is generally associated with a high chemical reactivity and low kinetic stability. Pictorial representation of HOMO and LUMO orbitals have been obtained from the optimized molecular geometry of MBZ-N using Gauss View software. Simulated HOMO, LUMO orbitals and HOMO-LUMO band gap are given in Figure 5. From the Figure 5, it can be seen that in HOMO, electron density is mainly spread over benzene rings while in LUMO, maximum electron density is seen over Nitrate group. Therefore, an electronic transition results in electron delocalization within the molecule. For titled molecule HOMO, LUMO energies and their gap have been calculated as -2.25425 eV, -0.09096 eV and 2.16329 eV respectively.

$$\text{HOMO energy (B3LYP)} = -2.25425 \text{ eV}$$

$$\text{LUMO energy (B3LYP)} = -0.09096 \text{ eV}$$

$$\text{Energy gap (HOMO - LUMO)} = 2.16329 \text{ eV}$$

On the basis of HOMO-LUMO energies global reactivity descriptors, such as the energies of frontier molecular orbitals (ϵ_{HOMO} , ϵ_{LUMO}), energy band gap ($\epsilon_{\text{HOMO}} - \epsilon_{\text{LUMO}}$), electronegativity (χ), chemical potential (μ), global hardness (η), global softness (S) and global electrophilicity index (ω); which describe the electrophilic behaviour, have been calculated for MBZ-N using Eqs. (1)-(5):

$$\chi = -1/2 (\epsilon_{\text{LUMO}} + \epsilon_{\text{HOMO}}) = 1.172605 \text{ eV} \quad (1)$$

$$\mu = -\chi = -1/2 (\epsilon_{\text{LUMO}} + \epsilon_{\text{HOMO}}) = -1.172605 \text{ eV} \quad (2)$$

$$\eta = 1/2(\epsilon_{\text{LUMO}} - \epsilon_{\text{HOMO}}) = 1.081645 \text{ eV} \quad (3)$$

$$S = 1/2\eta = 0.46225887(\text{eV})^{-1} \quad (4)$$

$$\omega = \mu^2 / 2\eta = 0.6356071 \text{ eV} \quad (5)$$

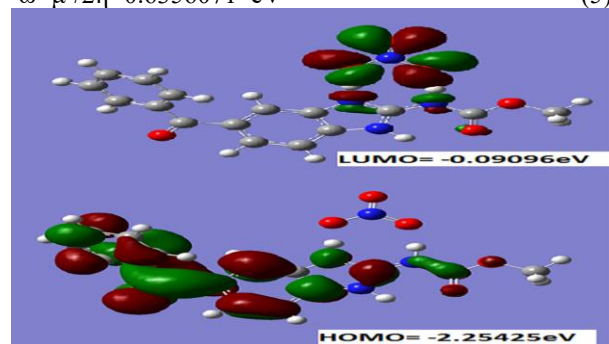


Figure 5. The frontier molecular orbitals of MBZ-N.

3.6. Molecular Docking

Molecular docking studies play an important role in knowing the binding interactions between a ligand and its receptor. Docking studies were carried out using Discovery studio visualiser, MGL tools [22], and AutoDock Vina[13] software. In the computations, both the ligand and receptor; Tyrosine-protein kinase ABL in the present case, in pdb (protein data bank) formats were prepared and used for docking. Molecular docking positions (grid positions) for MBZ ligand was taken as $40 \times 40 \times 40 \text{ \AA}^3$. According to the rotatable bonds of the ligand, nine poses were superposed with different affinity. Calculated affinity energy values, root mean square (RMS) values are given in Table 4.

Table 4. AutoDockVina results of the binding affinity and RMSD values of different poses.

MODES	Affinity kcal/mol	Rms dl.b	Rms du.b
1	-7.7	0.000	0.000
2	-7.7	12.251	14.483
3	-7.5	21.911	23.029
4	-7.4	16.467	19.863
5	-7.3	3.847	5.101
6	-7.1	3.274	8.049
7	-7.1	4.612	8.910
8	-7.1	4.299	8.429
9	-7.1	8.027	12.91

Best docking pose with a binding energy -7.7 kcal/mol between ligand and receptor, obtained using MGL tools software [22], is shown in Figure 6 (a). In Figure 6 (b), a closer view of interactions of the MBZ-N ligand with amino acids of target protein showing Hydrogen bonding interactions of ligand with different Aminoacids of the target protein along with the receptor surface drawn around the target protein is presented. Large affinity value of -7.7 kcal/mol confirms strong biological activity of MBZ-N ligand with protein and its possible potential application as a drug.

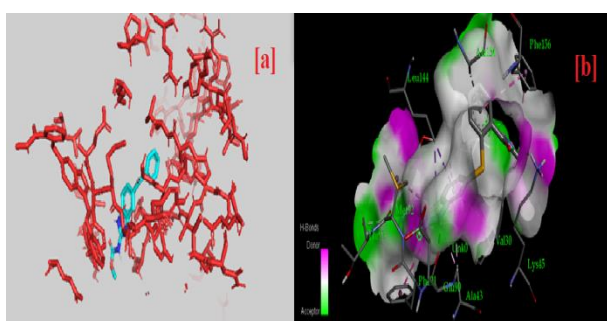


Figure 6.(a) Best docking pose between MBZ-N ligand and Tyrosine-protein kinase ABL enzyme. (b) Hydrogen bonding interaction of ligand with different Aminoacids of the target protein along with the receptor surface drawn around the target protein.

4. CONCLUSION

In this study, computational investigations on the structure, vibrational spectra and molecular reactivity descriptors such as natural bond analysis (NBO), HOMO-LUMO, and Molecular Electrostatic Potential (MEP) of MBZ-N molecule was done. The detailed PED analysis made possible an unambiguous assignments of the modes in vibrational spectra. The molecular reactivity analysis of NBO, HOMO-LUMO and MEP gave an insight into the possible biological activities.

Molecular docking study of the MBZ-N molecule with Tyrosine-protein kinase ABL has shown strong ligand receptor activity which confirms the pharmacological application of MBZ-N molecule. Therefore, we conclude that the title compound is an attractive molecule for future experimental as well as theoretical studies for medicinal and pharmacological applications.

ACKNOWLEDGEMENT

Authors would like to acknowledge the computational facilities provided by the Department of Physics, Chaudhary Charan Singh University, Meerut, during this work. Authors would also like to thank Prof. Beer Pal Singh, HOD Physics for encouragement and support.

DECLARATION OF ETHICAL STANDARDS

The author(s) of this article declare that the materials and methods used in this study do not require ethical committee permission and/or legal-special permission.

AUTHORS' CONTRIBUTIONS

Akansha TYAGI: Performed calculation, analyse the results and manuscript draft

Anuj KUMAR: Conceptualization, analyse the results, guidance and manuscript finalization

CONFLICT OF INTEREST

There is no conflict of interest in this study.

REFERENCES

- [1] FerreiraF.F., Antonio GutierrezS., Pires RosaP.C., Paiva-SantosC. de O., Crystal structure determination of mebendazole form a using high-resolution synchrotron x-ray powder diffraction data, *Int. J. Drug Dev. Res.*, 3: 26-33,(2011).
- [2] World Health Organization, WHO 19th Model List of Essential Medicines (April 2015) (Amended November 2015), (2015).
- [3] HimmelreichM., RawsonB. J., WatsonT. R., Polymorphic forms of mebendazole, *Aust. J. Pharm. Sci.*, 6 (4): 123-125,(1977).
- [4] SwanepoelE., LiebenbergW., DevarakondaB., De VilliersM.M., Developing a discriminating dissolution test for three mebendazole polymorphs based on solubility differences, *Pharmazie*, 58:117-12, (2003).

- [5] De VilliersM.M., TerblancheR.J., LiebenbergW., SwanepoelE., DekkerT.G., SongM.,Variable-temperature X-ray powder diffraction analysis of the crystal transformation of the pharmaceutically preferred polymorph C of mebendazole, *J. Pharm. Biomed. Anal.*, 38: 435-441,(2005).
- [6] BlatonN.M., PeetersO.M., DeranterC., (5-Benzoyl- 1H-benzimidazol-2-yl)-carbamic acid methyl ester hydrobromide (mebendazole\$HBr), C16H14BrN3O3, *Cryst. Struct. Commun.*, 9 (1): 181-186, (1980).
- [7] BrusauE.V., CamiG.E., NardaG.E., CuffiniS., AyalaA.P., J. Ellena, Synthesis and characterization of a new mebendazole salt: mebendazole hydrochloride, *J. Pharm. Sci.*, 97: 542-552,(2008).
- [8] ChenJ., LuT., New crystalline forms of mebendazole with n-alkyl carboxylic acids: neutral and ionic status, *Chin. J. Chem.*, 31: 635-640,(2013).
- [9] Guti_erreza E. L., SouzaM.S., Diniz L. F., Ellena J., Synthesis, characterization and solubility of a new anthelmintic salt: Mebendazole nitrate, *Journal of Molecular Structure*, 1161: 113-121,(2018).
- [10] Frisch M. J. and Trucks G. W. et. al. GAUSSIAN 09, Revision, Gaussian, Inc., Wallingford, CT, (2010).
- [11] Martin J.M.L. and AlsenoyC. V., Gar2ped, University of Antwerp, (1995).
- [12] PulayP., FogarasiG., Pang F. and BoggsJ.E., Systematic ab initio gradient calculation of molecular geometries, force constants, and dipole moment derivatives, *J. Am. Chem. Soc.*, 101(10): 2550-2560,(1979).
- [13] TrottO., OlsonA. J., Auto Dock Vina: improving the speed and accuracy of docking with a new scoring function, efficient optimization, and multithreading, *Journal Of Computational Chemistry*, 31(2):455-46,(2010).
- [14] ClarkR. J. H., and HesterR. E., Biomedical Applications of Spectroscopy, Wiley, Chichester, UK, (1996).
- [15] LiR., DhankharD., ChenJ., KrishnamoorthiA., CesarioT.C., RentzepisP. M., Identification of Live and Dead Bacteria: A Raman Spectroscopic Study, in IEEE Access, 7:23549-23559,(2019).
- [16] LiZ., XiaL., LiG. et al., Raman spectroscopic imaging of pH values in cancerous tissue by using polyaniline@gold nanoparticles. *Microchim Acta*, 186: 162(2019).
- [17] HuF., ShiL., MinW., Biological imaging of chemical bonds by stimulated Raman scattering microscopy. *Nat Methods*, 16: 830–842,(2019).
- [18] Lazaro-Pacheco D., Shaaban A.M., Rehman S., Rehman I., Raman spectroscopy of breast cancer, *Journal Applied Spectroscopy Reviews*, 55(6): 439-475,(2020).
- [19] Maurya A., Rastogi S., Rouillé G., Huisken F., and Henning T., *Astrophysical Journal*, 755:120(2012).
- [20] Szafran M., Komasa A., AdamskaE.B., *J. Mol. Struct. (Theochem.)* 827: 101-107, (2007).
- [21] Pathak S., Kumar A., Tandon P., Molecular structure and vibrational spectroscopic investigation of 4-chloro-4' dimethylamino-benzylidene aniline using density functional theory, 981: 1-9,(2010).
- [22] MorrisG. M., Huey R., LindstromW., SannerM. F., BelewR. K., GoodsellD.S., and OlsonA.J., Autodock4 and AutoDockTools4: automated docking with selective receptor flexibility. *J. Computational Chemistry*, 16: 2785-91,(2009).